Possible Mott transition in layered $Sr_2Mn_3As_2O_2$ single crystals

Chih-Wei Chen,[1] Weiyi Wang,[1] Vaideesh Loganathan,[1] Scott V. Carr,[1] Leland W. Harriger,[2] C. Georgen,[1] Andriy H. Nevidomskyy,[1] Pengcheng Dai,[1] C.-L. Huang,[1] and E. Morosan[1,*]

[1]*Department of Physics and Astronomy, Rice University, Houston, Texas 77005, USA*

[2]*NIST Center for Neutron Research, National Institute of Standards and Technology, Gaithersburg, Maryland 20899, USA*

(Received 8 April 2018; revised manuscript received 22 February 2019; published 24 April 2019)

Single crystals of $Sr_2Mn_3As_2O_2$ have been grown for the first time, for which we show a possible layer-selective Mott insulator behavior. This compound stands out as a hybrid structure of MnO_2 and MnAs layers, analogously to the active CuO_2 and FeAs layers, respectively, in the cuprate and iron-based high-temperature superconductors. Electrical transport, neutron diffraction measurements, together with density functional theory calculations on $Sr_2Mn_3As_2O_2$ single crystals converge toward a picture of independent magnetic order at $T_1 \sim 79$ K and $T_2 \sim 360$ K for the two Mn sublattices, with insulating behavior at odds with the metallic behavior predicted by calculations. Furthermore, our inelastic neutron-scattering studies of spin-wave dispersions for the Mn(1) sublattice reveal an effective magnetic exchange coupling of $SJ \sim 3.7$ meV. This is much smaller than those for the Mn(2) sublattice.

DOI: 10.1103/PhysRevB.99.144423

I. INTRODUCTION

The parent compounds of copper oxide and iron pnictide high-temperature superconductors (HTSs) are antiferromagnets, with the former Mott insulators with two-dimensional (2D) CuO_2 layers and the latter poor metals with nearly 2D FeAs layers. High T_c superconductivity occurs precisely in these layers on doping to suppress the antiferromagnetic (AF) order [1]. In a few cases, unconventional superconductivity has also been linked to orbital-selective Mott transitions. Here we show that combining the two types of active layers in $Sr_2Mn_3As_2O_2$ results in a layer-selective Mott insulator. The structural superposition of the two known HTSs and the underlining Mott physics are already promising premises for searching for unconventional superconductivity, with additional prospects arising from replacing Mn with Cu and Fe in the respective layers. The main outcomes of this study, *only* possible with the first growth of single crystals of $Sr_2Mn_3As_2O_2$, are as follows: (i) We characterize the nearly independent AF order at the two Mn sites, confirming the reported 3D AF order in the MnAs layer; (ii) single-crystal neutron scattering resolves the Mn(1) quasi-2D ordering in the MnO_2 layer, essential for explaining the observed insulating behavior; (iii) we find effective magnetic exchange coupling of the Mn(2) sublattice much larger than for Mn(1), exceeding the expectation from the relative ordering temperatures; (iv) density functional theory (DFT) suggests a Mott state above T_1, with possible orbital selectivity, where the $d_{x^2-y^2}$ orbital in the MnO_2 layer plays the dominant role, analogously to cuprates. As a realization of an orbital-selective Mott insulator, $Sr_2Mn_3As_2O_2$ offers opportunities to induce unconventional superconductivity, metal-to-insulator transitions, or colossal magnetoresistance.

II. EXPERIMENTAL METHODS

The $Sr_2Mn_3As_2O_2$ single crystals and polycrystalline sample preparation, as well as the details of DFT and DFT+U calculations, are included in the Supplemental Material [2]. Magnetization and electrical resistivity were measured using Quantum Design MPMS and PPMS instruments. Neutron scattering was performed on single crystals in SPINS at NIST. For elastic single-crystal neutron scattering, a 50-mg crystal was used. For inelastic neutron scattering, 30 single-crystal pieces (1 g in total) were coaligned with mosaic within 5°. The measurements were performed in the (H0L) and (HHL) planes for $T = 15$–390 K controlled by a Closed Cycle Refrigerator. A BeO filter was placed after the sample to remove higher-order scattering. The final energy was selected as 5 meV.

III. RESULTS AND DISCUSSIONS

The $Sr_2Mn_3As_2O_2$ crystal structure [Fig. 1(a)] consists of a heterogeneous stacking of "CuO_2"-type $Mn(1)O_2$ layers (red-yellow) and "FeAs"-type Mn(2)As layers (blue-green) [3,4]. Our neutron diffraction data confirm the already-known Mn(2) magnetic structure [4,5] and resolve the previously unknown Mn(1) structure, with the latter only possible with the availability of single crystals. The Mn(2) moments form a long-range G-type AF order (antiparallel spin alignment in all three crystallographic directions) with the moments along c. In contrast to the 3D magnetic order at the Mn(2) site, Mn(1) undergoes a quasi-2D short-range AF order [Fig. 1(b)], with the moments along a, reminiscent of the spin configuration of $YBa_2Cu_3O_{6+x}$ [6,7]. The remarkable consequence of this magnetic structure is an independent magnetic order taking place at the two Mn sites, with their AF Bragg peak positions in reciprocal space shown in Figs. 1(c) and 1(d). This conclusion is corroborated by DFT calculations, showing that, on magnetic ordering in the Mn(2)As

*emorosan@rice.edu

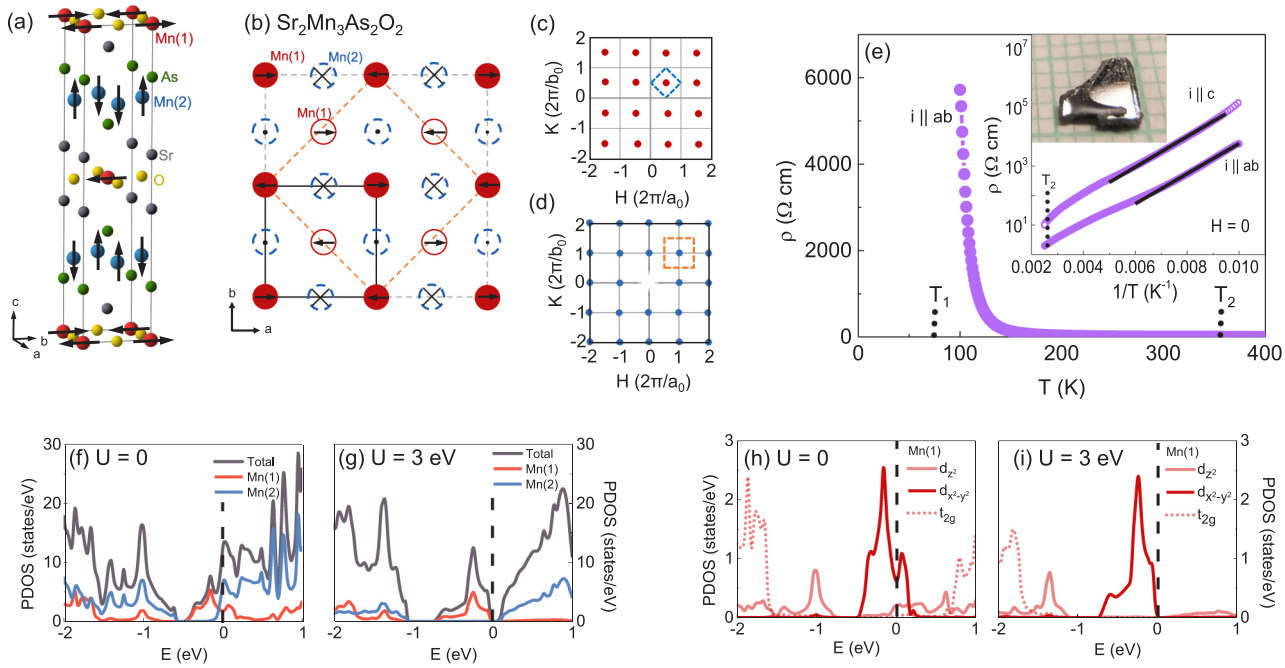

FIG. 1. (a) $Sr_2Mn_3As_2O_2$ crystal structure with black arrows indicating the direction of magnetic moments. (b) The *ab*-plane magnetic structure, with solid and open circles indicating Mn ions in different layers. The reciprocal lattice of the (c) Mn(1) and (d) Mn(2) magnetic structure. (e) The temperature-dependent resistivity of $Sr_2Mn_3As_2O_2$, with a semilog plot as a function of $1/T$ shown in the inset, together with low-T linear fits (solid lines) and a crystal picture on an mm grid shown in the upper left corner. Density of states near Fermi energy (f) without considering Coulomb interaction and (g) with Coulomb interaction of 3 eV. [(h) and (i)] Partial density of states at Mn(1) sites for individual orbitals, d_{z^2}, $d_{x^2-y^2}$, and t_{2g}, without considering Coulomb interaction and with Coulomb interaction of 3 eV.

layer, the Mn(2) density of states (DOS) at the Fermi level (E_F) is drastically suppressed to become nearly insulating [Fig. 1(f) and Fig. S1]. By contrast, Mn(1)O_2 remains metallic, unless a sufficiently large value of Hubbard U is included in calculations, at which point the gap opens up [Fig. 1(g) and Figs. S1(e) and S1(f)]. This layer-selective metal-insulator transition is consistent with the transport measurements, which indicate that insulating behavior occurs well below T_2, closer to T_1 when Mn(1) orders magnetically [Fig. 1(e)]. To elucidate the nature of this insulating state, we analyzed the orbital composition of the Mn(1) layer, concluding that, in the absence of U, two E_g orbitals ($d_{x^2-y^2}$ and d_{z^2}) contribute to DOS(E_F) [Fig. 1(h) and Fig. S2]. On increasing the Hubbard repulsion, an orbital-selective Mott transition takes place, with the d_{z^2} orbital becoming insulating first at $U \approx 2$ eV [Fig. S2(f)], followed by a Mott transition in the $d_{x^2-y^2}$ orbital for $U \gtrsim 3$ eV [Fig. 1(i) and Fig. S2(h)]. This is akin to the theoretical prediction in $Ca_{2-x}Sr_xRuO_4$ [1], and experimental confirmation through optical measurements in $Sr_2Mn_3As_2O_2$ is currently underway.

In order to resolve the magnetic structure on the two independent Mn sublattices, and to verify the layer-selective magnetism, we conducted single-crystal neutron scattering. Previous neutron powder diffraction [4,5] suggested that Mn(2) had a G-type AF order with the magnetic moment along c [Fig. 1(a)] and that Mn(1) had the same type of magnetic order at a lower temperature T_1. A closer look at the crystal structure [Fig. 1(b)] indicates a staggered stacking of the square Mn(1)-O layers (solid, open red circles in $z = 0$, 1/2 planes), with the parallel-stacked square Mn(2)-As layers (open dashed circles). The corresponding diffraction spots of the Mn(1) and Mn(2) sites in the reciprocal lattice and the Brillouin zones of both sites are shown in Figs. 1(c) and 1(d). As the neutron data below indicate, the magnetic moments are aligned antiparallel with their nearest neighbors within each layer, confirming the previously known Mn(2) AF order along c. However, we find that the Mn(1) ions order antiferromagnetically within the *ab*-plane, in stark contrast to the prediction from powder neutron diffraction.

The transport properties appear to be dominated by the Mn(1) sublattice. The resistivity increases on cooling, with no visible signature of the transition at $T_2 \sim 360$ K [marked by the vertical line in Fig. 1(e)]. On further cooling, a second transition had been reported around $T_1 \sim 79$ K [4], and our elastic neutron-scattering data (Fig. 2) show that this is associated with the ordering of the Mn(1) moments. However, at temperatures substantively above T_1 [vertical line, Fig. 1(e)], the resistivity diverges on cooling, with an energy gap around 100 meV determined from the linear fit of $\ln\rho$ vs. $1/T$ [solid lines, Fig. 1(e), inset], a value close to that reported for polycrystalline samples [4]. While the gap appears nearly isotropic, the c axis resistivity is about two orders of magnitude larger than the one within the *ab*-plane, which suggests higher probability for electrons hopping *within* the plane than between planes, similar to those of copper oxides.

Further insight into the behavior of $Sr_2Mn_3As_2O_2$ is offered by the electronic band structure calculations using the DFT+U method. Both Mn(1) and Mn(2) ions are found to be in the +2 (d^5) oxidation state, with zero orbital moment and effective spin $S = 5/2$. The comparison of the ground-state

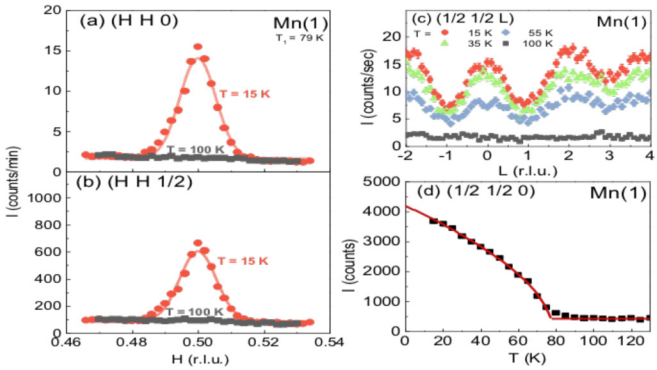

FIG. 2. (a) Low-temperature ($T = 15$ K) and (b) high-temperature ($T = 100$ K) neutron intensity data, with in-plane wave-vector scan around Mn(1) site: $[\frac{1}{2}\ \frac{1}{2}\ 0]$ and $[\frac{1}{2}\ \frac{1}{2}\ \frac{1}{2}]$ (c) Wave-vector scan perpendicular to the *ab*-plane around the Mn(1) site. (d) Mn(1) order parameter scan.

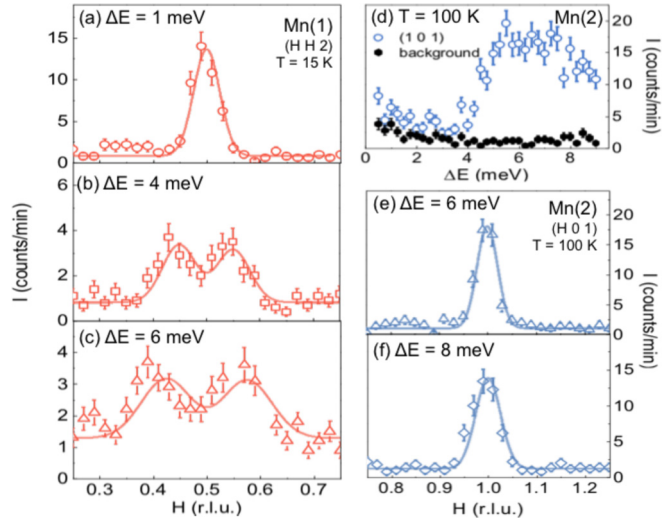

FIG. 3. [(a)–(c)] Mn(1) constant energy scans. (d) Mn(2) energy scan. [(e)–(f)] Mn(2) constant energy scans.

energies of the paramagnetic (PM), AF, and hypothetical ferromagnetic (FM) configurations show that the AF state is energetically more favorable both in DFT and DFT+U. Moreover, DFT predicts that the AF state is metallic, as illustrated in Fig. 1(f), contrary to the experimental findings. This indicates that the electron interactions play an important role in $Sr_2Mn_3As_2O_2$. To account for electron-electron interactions, we performed a series of DFT+U calculations and found that a spectral gap opens up at E_F for values of the Hubbard interaction starting at $U_c \approx 3$ eV. The DOS for $U = 3$ eV is shown in Fig. 1(g), exhibiting a spectral gap of $\sim$0.1 eV, in agreement with the charge gap estimated from the transport measurements [Fig. 1(e)]. The theoretical value of the ordered moment on Mn(2) is close to 4 μ_B, in agreement with the current and previous neutron-scattering data [4,5].

The projected DOS analysis in Figs. 1(f) and 1(g) leads us to conclude that the Mn(2) layer is nearly insulating due to the formation of the AF long-range order below T_2, whereas the Mn(1) layer remains metallic and only develops a spectral gap below its ordering temperature T_1, provided U is sufficiently high (above $U_c \approx 3$ eV). The constrained DFT calculation [8] yields the value of Hubbard U on Mn(1) site $U \approx 5.7$ eV, which is admittedly on a higher side compared to the typical values that usually do not exceed 4 eV in Mn compounds (see, e.g., Table II in Ref. [9]). Nevertheless, while the value of U may not be quantitatively correct, qualitatively it is above the threshold of $U_c \approx 3$ eV where our analysis indicates the onset of the Mott transition. We thus conclude that $Sr_2Mn_3As_2O_2$ harbors a layer-selective Mott phase, with the cuprate-type MnO_2 layer playing a key role in the electronic properties. Further analysis reveals that the dominant states near the Fermi level come from the Mn(1) $d_{x^2-y^2}$ orbital [Figs. 1(h) and 1(i) and Fig. S2], akin to the cuprate HTSs.

A determination of the magnetic structure at the Mn(1) site can reveal the role of the magnetism in the cuprate-like layer in the layer-selective transport properties of $Sr_2Mn_3As_2O_2$. The theoretical DFT and DFT + U calculations predict the lowest energy state to be an AF in-plane spin configuration, with wave vector $Q = (\frac{1}{2}\ \frac{1}{2}\ 0)$ and a corresponding $\sqrt{2} \times \sqrt{2}$ doubling of the unit cell in the *ab*-plane. Because of the ABAB stacking of the Mn(1) planes, the out-of-plane ordering of Mn(1) spins is ambiguous. Our elastic neutron-scattering measurements indeed find a peak at $(\frac{1}{2}\ \frac{1}{2}\ 0)$ and equivalent positions, corroborating the theoretically predicted in-plane AF order, with the magnetic moment along a. Additional elastic scans of the $(\frac{1}{2}\ \frac{1}{2}\ 0)$ peak were performed along $[HH0]$ [Fig. 2(a)] and $[00L]$ [Fig. 2(c)]. In Figs. 2(a) and 2(b), $(\frac{1}{2}\ \frac{1}{2}\ 0)$ and equivalent positions show a peak at $T = 15$ K, which disappears at $T = 100$ K, suggesting that it is associated with the Mn(1) magnetic order below 100 K. The spin-spin correlation lengths along $[HH0]$ and $[00L]$, estimated by the full width at half maximum of the magnetic peak, are around 430 Å and 13 Å, respectively. The larger in-plane vs. out-of-plane correlation length suggests that the Mn(1) magnetic order is quasi-2D, with a substantial correlation length. The transition temperature T_1 is precisely determined by an order parameter scan on the $(\frac{1}{2}\ \frac{1}{2}\ 0)$ peak [Fig. 2(d)]. The magnetic scattering intensity decrease with increasing temperature is best fit with $I = I_0(1 - \frac{T}{T_1})^{2\beta}$ [line, Fig. 2(d)], which yields the transition temperature $T_1 \sim 79$ K and critical exponent $\beta \sim 0.55$ close to the mean-field prediction of 0.5 [10]. By comparison, similar fits around the Mn(2) ordering yield $T_2 = 360$ K and $\beta = 0.32$ (Supplemental Material [2]). In this case, β is close to the theoretical value for a 3D Ising model $\beta = 0.326$ [10]. Given that the order of Mn(1) moments is highly anisotropic, with weakly coupled antiferromagnetic planes, one expects the critical exponents to reflect a 2D-to-3D crossover. Moreover, Mn moments likely have an itinerant character, in which case this crossover was suggested to result in mean-field exponents in certain cases [11], perhaps explaining the mean-field character of our measured value of $\beta = 0.55$.

After determining the magnetic structure in the Mn-O layer, we carried out inelastic neutron-scattering measurements to study the magnetic excitations in $Sr_2Mn_3As_2O_2$. An energy scan on the Mn(1) site (Fig. S4) at $T = 15$ K reveals that the spin waves are gapless. Several constant energy scans were performed at $T = 15$ K [Figs. 3(a)–3(c)

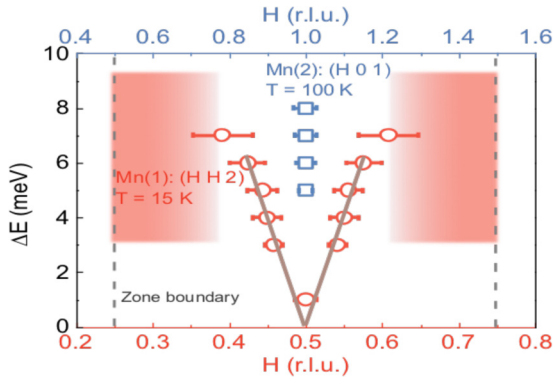

FIG. 4. Magnetic dispersion derived from constant energy scans for both Mn(1) (squares) and Mn(2) (circles). The shade area indicates zones close to the phase boundary where the signal becomes weak.

and Supplemental Material [2]] to search for the spin wave at Mn(1). For higher energy transfer ($\Delta E > 3$ meV), scans around $(\frac{1}{2}\ \frac{1}{2}\ 2)$ peak split into two counterpropagating spin waves. By contrast, an energy scan of the (101) peak on the Mn(2) site at $T = 100$ K [Fig. 3(d)] suggests the presence of a magnetic gap of ∼4 meV. Several constant energy scans with energy transfer larger than the gap ($\Delta E > 4$ meV) were performed at $T = 100$ K [Figs. 3(e) and 3(f)]. No splitting was observed up to the highest measured energy transfer (8 meV), an indication that the stiffness of the spin wave at Mn(2) site is much higher than that for Mn(1).

The spin-wave dispersion of both Mn(1) and Mn(2) is displayed in Fig. 4. The Mn(2) dispersion was measured at 100 K, higher than T_1, to avoid the signal from Mn(1). When the wave vector is close to the elastic peak position $(\frac{1}{2}\ \frac{1}{2}\ 2)$, the energy dispersion of an AF spin wave at low energy is expected to be linear. The coupling strength between the magnetic moments can be derived from the slope of the linear fit of the dispersion curves (solid lines, Fig. 4). This gives the coupling constant $SJ \approx 3.7$ meV. The zero intercept further supports the scenario of gapless Mn(1) spin waves. At the Mn(2) site, although the peak width increases with increasing energy transfer, no splitting was observed up to the highest energy transfer (8 meV). This means that the effective magnetic exchange coupling of the Mn(2) sublattice is much larger than that of Mn(1).

These results point to the independent nature of magnetic ordering at the Mn(1) and Mn(2) sites. Moreover, the theoretical calculations indicate that, on magnetic ordering below T_2, the Mn(2)As layer becomes nearly insulating and effectively decouples from the rest of the system provided $U \gtrsim 2$ eV [Fig. 1(f) and Fig. S1]. As a result of this layer-selective metal-insulator transition, the low-temperature electronic properties are solely determined by the $Mn(1)O_2$ layer, isostructural to the CuO_2 layer in HTSs. Of course there are significant differences with the latter, because Mn^{2+} has five d electrons, and Hund's coupling plays a crucial role in quenching the orbital moment and resulting in an effective spin-5/2. Nevertheless, the Mn(1) d-bands are strongly correlated and our theoretical calculations point to orbital-selective physics at play in this material. Indeed, we find that, as a result of Hund's coupling, the three t_{2g} orbitals are completely spin polarized, forming a so-called half-metal and not participating in the DOS at the Fermi level. The remaining two e_g orbitals ($d_{x^2-y^2}$ and d_{z^2}) undergo a metal-insulator transition at different values of Hubbard U (Fig. S2), thus realizing an orbital-selective Mott state for $2.0 \lesssim U \lesssim 3.0$ eV where only the Mn(1) $d_{x^2-y^2}$ orbital remains metallic.

The idea of an orbital-selective Mott transition was first proposed to explain the ground state and transport properties of $Ca_{1-x}Sr_xRuO_4$ [12]. The transport properties in $Sr_2Mn_3As_2O_2$ are also significantly affected by the orbital-selective Mott phase in specific orbitals. Furthermore, it is expected that other properties such as superconductivity and magnetism are also affected by the orbital-selective Mott phase [12–14], e.g., the unconventional superconductivity in certain iron-based superconductors [15,16], the magnetism in La_2CuO_4 [17], where the antiferromagnetism is caused by splitting due to a Mott transition and the half-occupancy of the $d_{x^2-y^2}$ orbital. In $Sr_2Mn_3As_2O_2$, it is the combination of Hund's coupling and Hubbard repulsion that drives the possible orbital-selective Mott transition in the $Mn(1)O_2$ layer. Once the critical value of $U_c \approx 3$ eV is reached, both e_g orbitals become insulating below T_1; however, unlike typical Mott insulators with large spectral gap of order U, we find an indirect modest gap 0.1 eV of charge-transfer type between the top of Mn(1) $d_{x^2-y^2}$ lower Hubbard band at the X point and the bottom of the Mn(2) t_{2g} upper Hubbard band at the Γ point. By contrast, the direct gap between the lower and upper Hubbard bands within the same orbital is sizable, of order U. We therefore have a theoretical scenario that supports the idea of an orbital-selective Mott transition, and experimental verification from ARPES is ongoing.

IV. CONCLUSIONS

In summary, our neutron-scattering experiments have conclusively determined the magnetic structure of $Sr_2Mn_3As_2O_2$. The two magnetic transitions at T_2 and T_1 occur in different layers and are decoupled from each other, characterized by different critical exponents. Inelastic neutron scattering concludes that Mn(1) has gapless spin waves compared to a 4-meV spin gap when Mn(2) orders at T_2. We find that the Mott transition in $Sr_2Mn_3As_2O_2$ is layer selective, and potentially orbital selective, where the Mn $d_{x^2-y^2}$ orbital in Mn(1)-O layer dominates the electronic DOS at E_F. DFT + U calculations suggest that, while the MnAs layer develops a gap at E_F first due to the onset of AF order at T_2, the MnO_2 layer, isostructural to the cuprates, only develops a spectral gap when the Hubbard U is sufficiently high (above ∼3 eV). It turns out that the analogy with the Mott-insulating parent compounds of the cuprates goes beyond simply the structural similarity: Akin to the cuprates [18], the $Sr_2Mn_3As_2O_2$ band calculations confirm that the key player is the Mn(1) $d_{x^2-y^2}$ orbital, which lies close to E_F and undergoes a Mott transition. The multiorbital character of the Mn^{2+} ions is different from that of Cu^{2+}, with Hund's coupling playing a crucial role in the opening of a spectral gap in the spin-polarized t_{2g} orbitals. Nevertheless, the $Sr_2Mn_3As_2O_2$ ground state is not a "Hund's metal" like the iron pnictides [19]; rather, a true Mott transition takes place below the ordering temperature of the Mn(1)

layer, as in the parent compounds of the cuprates. It would be desirable for future theoretical studies to investigate the nature of the proposed layer-selective Mott transition using more advanced methods such as dynamical mean-field theory (DMFT) [20]; however, one has to be mindful of the fact that there are two inequivalent Mn sites in the unit cell (1 in MnO_2 layer and 2 in MnAs layer) and that all five $3d$ orbitals of each Mn atom cross the Fermi level in the paramagnetic state, making DMFT calculations challenging.

Despite extensive theoretical study of the orbital-selective Mott transition [13–15] and its correlation with unconventional superconductivity [16], only a very limited number of orbital-selective Mott insulators have been proposed, including $A_xFe_{2-y}Se_2$ [15,21] and $Ca_{1.8}Sr_{0.2}RuO_4$ [12,22–24]. If confirmed experimentally, the new orbital-selective Mott insulator $Sr_2Mn_3As_2O_2$ reported in this work may result in unconventional superconductivity, insulator-to-metal transition, and perhaps colossal magnetoresistance on electron or hole doping.

ACKNOWLEDGMENTS

C.-W.C., C.G., C.-L.H., and E.M. acknowledge support from the Gordon and Betty Moore Foundation's EPiQS initiative through Grant No. GBMF 4417. The theoretical work by V.L. and A.H.N. was supported by the Welch Foundation Grant No. C-1818. A.H.N. also acknowledges support from the National Science Foundation Grant No. DMR-1350237. The neutron-scattering work by P.D. is supported by the United States DOE, BES, through Contract No. DE-SC0012311. Part of the work at Rice University is supported by the Robert A. Welch Foundation through Grant No. C-1839 (P.D.).

[1] P. Dai, Antiferromagnetic order and spin dynamics in iron-based superconductors, Rev. Mod. Phys. **87**, 855 (2015).

[2] See Supplemental Material at http://link.aps.org/supplemental/10.1103/PhysRevB.99.144423 for details of the synthesis, DFT calculations, and experiments.

[3] T. C. Ozawa and S. M. Kauzlarich, Chemistry of layered d-metal pnictide oxides and their potential as candidates for new superconductors, Sci. Technol. Adv. Mater. **9**, 033003 (2008).

[4] R. Nath, V. O. Garlea, A. I. Goldman, and D. C. Johnston, Synthesis, structure, and properties of tetragonal $Sr_2M_3As_2O_2$ ($M_3 = Mn_3$, Mn_2Cu, and $MnZn_2$) compounds containing alternating CuO_2-type and FeAs-type layers, Phys. Rev. B **81**, 224513 (2010).

[5] S. L. Brock, N. P. Raju, J. E. Greedan, and S. M. Kauzlarich, The magnetic structures of the mixed layer pnictide oxide compounds $Sr_2Mn_3Pn_2O_2$ (Pn = As, Sb), J. Alloys Compd. **237**, 9 (1996).

[6] J. M. Tranquada *et al.*, Neutron-Diffraction Determination of Antiferromagnetic Structure of Cu Ions in $YBa_2Cu_3O_{6+x}$ with $x = 0.0$ and 0.15, Phys. Rev. Lett. **60**, 156 (1988).

[7] P. Burlet, J. Henry, and L. Regnault, In-plane magnetic anisotropy in antiferromagnetic $YBa_2Cu_3O_{6+x}$, Physica C **296**, 205 (1998).

[8] G. K. H. Madsen and P. Novak, Charge order in magnetite: An LDA+U study, Europhys. Lett. **69**, 777 (2005).

[9] E. Şaşsioğlu, I. Galanakis, C. Friedrich, and S. Blügel, Ab initio calculation of the effective on-site Coulomb interaction parameters for half-metallic magnets, Phys. Rev. B **88**, 134402 (2013).

[10] S. Blundell, *Magnetism in Condensed Matter* (Oxford University Press, Oxford, 2001)

[11] A.-M. Daré, Y. M. Vilk, and A.-M. S. Tremblay, Crossover from two- to three-dimensional critical behavior for nearly antiferromagnetic itinerant electrons, Phys. Rev. B **53**, 14236 (1996)

[12] V. I. Anisimov, I. A. Nekrasov, D. E. Kondakov, T. M. Rice, and M. Sigrist, Orbital-selective Mott-insulator transition in $Ca_{2-x}Sr_xRuO_4$, Eur. Phys. J. B **25**, 191 (2002).

[13] L. de'Medici, A. Georges, and S. Biermann, Orbital-selective Mott transition in multiband systems: Slave-spin representation and dynamical mean-field theory, Phys. Rev. B **72**, 205124 (2005).

[14] S. Biermann, L. de' Medici, and A. Georges, Non-Fermi-Liquid Behavior and Double-Exchange Physics in Orbital-Selective Mott Systems, Phys. Rev. Lett. **95**, 206401 (2005).

[15] R. Yu and Q. Si, Orbital-Selective Mott Phase in Multiorbital Models for Alkaline Iron Selenides $\mathbf{K}_{1-x}Fe_{2-y}Se_2$, Phys. Rev. Lett. **110**, 146402 (2013).

[16] L. de'Medici, G. Giovannetti, and M. Capone, Selective Mott Physics as a Key to Iron Superconductors, Phys. Rev. Lett. **112**, 177001 (2014).

[17] P. Fulde, *Electron Correlations in Molecules and Solids*, 3rd ed. (Springer-Verlag, Berlin, 1993).

[18] D. Pines, $d_{x^2-y^2}$ pairing and spin fluctuations in the cuprate superconductors: Experiment meets theory, Physica C **235-240**, 113 (1994).

[19] L. Fanfarillo and E. Bascones, Electronic correlations in Hund metals, Phys. Rev. B **92**, 075136 (2015).

[20] A. Georges, G. Kotliar, W. Krauth, and M. J. Rozenberg, Dynamical mean-field theory of strongly correlated fermion systems and the limit of infinite dimensions, Rev. Mod. Phys. **68**, 13 (1996).

[21] M. Yi, D. H. Lu, R. Yu, S. C. Riggs, J. H. Chu, B. Lv, Z. K. Liu, M. Lu, Y. T. Cui, M. Hashimoto, S. K. Mo, Z. Hussain, C. W. Chu, I. R. Fisher, Q. Si, and Z. X. Shen, Observation of Temperature-Induced Crossover to an Orbital-Selective Mott Phase in $A_xFe_{2-y}Se_2$(A = K, Rb) Superconductors, Phys. Rev. Lett. **110**, 067003 (2013).

[22] S. Nakatsuji and Y. Maeno, Quasi-Two-Dimensional Mott Transition System $Ca_{2-x}Sr_xRuO_4$, Phys. Rev. Lett. **84**, 2666 (2000).

[23] M. Neupane, P. Richard, Z.-H. Pan, Y.-M. Xu, R. Jin, D. Mandrus, X. Dai, Z. Fang, Z. Wang, and H. Ding, Observation of a Novel Orbital Selective Mott Transition in $Ca_{1.8}Sr_{0.2}RuO_4$, Phys. Rev. Lett. **103**, 097001 (2009).

[24] Y. Song *et al.*, A Mott insulator induced near iron pnictide superconductors, Nat. Commun. **7**, 13879 (2016).